

A CONSERVED INTERACTION BETWEEN TRANSFERRIN AND TRANSFERRIN-BINDING
PROTEINS FROM PORCINE PATHOGENS

Leslie P. Silva¹, Ronghua Yu², Charles Calmettes³, Xue Yang², Trevor F. Moraes³, Anthony B. Schryvers^{1,2}, and David C. Schriemer¹

Department of Biochemistry & Molecular Biology, University of Calgary, Calgary, Canada¹, Department of Microbiology & Infectious Diseases, University of Calgary, Calgary, Canada² and Department of Biochemistry, University of Toronto, Toronto, Canada³

Running Head: Transferrin interaction with porcine pathogen TbpBs

Address correspondence by email to ABS (schryver@ucalgary.ca) or DCS (dschriem@ucalgary.ca).

Gram-negative porcine pathogens from the *Pasteurellaceae* family possess a surface receptor complex capable of acquiring iron from porcine transferrin (pTf). This receptor consists of transferrin binding protein A (TbpA), a transmembrane iron transporter, and TbpB, a surface-exposed lipoprotein. Questions remain as to how the receptor complex engages pTf in such a way that iron is positioned for release, and whether divergent strains present distinct recognition sites on Tf. In this study, the TbpB-pTf interface was mapped using a combination of mass shift analysis and molecular docking simulations, localizing binding uniquely to the pTf C-lobe for multiple divergent strains of *Actinobacillus plueropneumoniae* and *suis*. The interface was further characterized and validated with site-directed mutagenesis. Although targeting a common lobe, variants differ in preference for the two sub-lobes comprising the iron coordination site. Sub-lobes C1 and C2 participate in high affinity binding, but sub-lobe C1 contributes in a minor fashion to the overall affinity. Further, the TbpB-pTf complex does not release iron independent of other mediators, based on competitive iron binding studies. Together, our findings support a model whereby TbpB efficiently captures and presents iron-loaded pTf to other elements of the uptake pathway, even under low iron conditions.

INTRODUCTION

Bacteria are dependent upon effective and efficient iron acquisition mechanisms in order to survive and proliferate in the iron-limited environment of the host (1-3). Pathogenic Gram-negative bacteria within the *Neisseriaceae* and

Pasteurellaceae families rely on specialized uptake systems to acquire iron directly from host iron-binding proteins (2-5). These bacteria can acquire iron from host transferrin (Tf) in particular (6), but in some cases also lactoferrin (7,8), and hemoglobin/haptoglobin (9). To understand such uptake mechanisms, a detailed characterization of relevant receptor-host protein interactions is required.

The bacterial transferrin receptors are comprised of two iron-repressible surface components, transferrin binding protein A (TbpA), a TonB-dependent integral outer membrane protein of approximately 100kDa and transferrin binding protein B (TbpB), a lipoprotein varying in size from 60-100kDa (2,3,5,10,11). They have been found in clinical isolates of the *Neisseriaceae*, *Pasteurellaceae* as well as the *Moraxellaceae* families (12), and constitute the outer membrane receptor complex responsible for binding transferrin and transporting iron across the outer membrane into the periplasmic space (4,13). These receptors exhibit a strict host-specificity. For example, receptors of porcine pathogens will specifically bind porcine transferrin (pTf) but not human, avian, bovine or ovine transferrin (14).

Tf is a glycoprotein of approximately 80kDa, composed of two highly homologous N and C-lobes (15). Each lobe contains two domains, connected by two antiparallel β -strands in a clamshell-like fold, producing a cleft that coordinates Fe^{3+} in the binding pocket, along with a synergistic anion (CO_3^{2-} or $\text{C}_2\text{O}_4^{2-}$) (16-18). Crystal structures of several full-length Tfs from different species reveal a significant conformational change upon iron binding, resulting in a closing of the cleft around the coordinated iron (19). Apo and holo-Tf forms have different affinities for the bacterial transferrin binding protein receptors. Unlike TbpA, the TbpBs

have a strong preference for binding to the holo form of Tf (20-23), which suggests that TbpB may play a role in efficient capture of the holo form of Tf (24,25). For the *Actinobacillus spp.*, *in vitro* studies have shown that a TbpB-deficient strain could utilize Tf-bound iron, but was avirulent (26). This potential for diverse receptor-transferrin recognition mechanisms provides a rationale for characterizing Tf-TbpB interactions across multiple variants. The sequence heterogeneity for TbpB proteins in particular is considerable, with 47-82% sequence identity observed in variants from a cross-section of pathogenic strains (25,27). Therefore, this study seeks to determine the impact of such heterogeneity on the interaction with Tf, from the perspective of Tf.

A survey of existing binding studies suggests that TbpB interacts with Tf through the receptor N-lobe (28) and the Tf C-lobe (11,22,29,30). Recent work by Ling *et al.* has described two TbpB variants from *Neisseria meningitidis* that interact with the C-lobe of human transferrin (hTf) (11), although it has been previously reported that both Tf lobes are involved in binding, specifically for *Moraxella catarrhalis* (23) and the ovine pathogen *Haemophilus paragallinarum* (30). By taking advantage of structural information available for divergent TbpBs from porcine pathogens (5,31), the current study was initiated to determine how the considerable variability in the TbpB surface regions maintain the interaction with pTf. Together with a companion study by Calmettes *et al.* (31), we provide a structural analysis of the receptor-Tf interaction representing several divergent porcine pathogenic strains, and evaluate the impact of iron loading on the molecular recognition mechanism in greater detail.

Recently available protein structures provide an opportunity to map interactions with pTf at high resolution, using a hybridized strategy based on mass shift mapping that involves hydrogen/deuterium exchange methods and structural modeling (32,33). Shift mapping was recently applied to hTf (11), however the absence of a reliable human pathogenic TbpB structure prevented a detailed characterization of the transferrin binding site. In the current study, shift mapping was used to locate interfaces and

altered dynamics upon the binding of pTf to four TbpB variants. This mapping data was used to test heterodimer models arising from computational docking of pTf to available TbpB structures (5,31). The models were further tested through mutations and surface plasmon resonance (SPR) binding studies, as guided by hot-spot analysis. Our findings reveal that all four receptor variants interact at a partially conserved interface on the C-lobe of transferrin and highlight how iron-loading renders the C-lobe uniquely capable of binding to TbpB.

EXPERIMENTAL PROCEDURES

Production of recombinant TbpB proteins

The mature coding region of TbpB from *A. pleuropneumoniae* strain *Aph49* (serotype7), *Aph87* (serotype 5), *Aph89* (serotype 1) and *A. suis* *AsH57* were PCR amplified and cloned in to the in-frame BamHI restriction site of a customized expression vector preceded by a polyhistidine region, a maltose binding protein and a tobacco etch virus (TEV) protease cleavage site. *E. coli* strain C43 cells transformed with the recombinant plasmids were grown in 1 liter of Luria base (LB) broth supplemented with ampicillin (100 µl/ml) for 20 hr at 37°C. Cells were harvested by centrifugation at 7,000 x g for 10 min, resuspended in 30 ml of resuspension buffer (50 mM NaCl, 50 mM Tris, pH 8.0). and lysed with a Emulsiflex cell homogenizer (Avestin Inc., Ottawa, Canada). The cell lysate was centrifuged at 40,000 x g for 20 min and the supernatant was applied to a Ni-NTA column to isolate the Mbp:TbpB fusion protein. After elution from the column and dialysis in buffer, the maltose binding protein (Mbp) tag was cleaved from the TbpBs by tobacco etch virus (TEV) protease digestion overnight, at room temperature. The digestion mixture was applied to a Ni-NTA column to remove the Mbp and his-tagged recombinant TEV. The purified TbpBs were dialyzed against 50 mM NaH₂PO₄, 0.3M NaCl, 5 mM imidazole, pH 8.0.

Production and purification of pTf

Recombinant pTfs were produced from a *Pichia pastoris* expression system, followed by iron-loading. Briefly, recombinant pTf expressed from a modified pPICαA vector (Invitrogen) in *Pichia pastoris* was precipitated from the culture supernatant by ammonium sulphate. After centrifugation the pellet was then resuspended in

water, and the solution dialyzed against 10 mM HEPES, pH 7.0, overnight at 4°C. The dialyzed solution was applied to a Q-Sepharose column, and eluted via an NaCl gradient. The purified solution was dialyzed against 10 mM HEPES, pH 7.0, and then analyzed by SDS-PAGE.

Site directed mutagenesis of pTf to generate R509A, D360A, and S625K mutations was performed using the Invitrogen Genear[®] Site Directed Mutagenesis System, as initially described by Weiner et al. (34). Expression of the mutants followed the same procedure as wildtype.

FbpA Protein production

Wild-type *Haemophilus influenzae* FbpA was expressed and iron-loaded as described by Shouldice et al. (35). To generate apo-FbpA, holo-FbpA was extensively dialyzed against 100mM sodium acetate, 100 mM sodium phosphate monobasic, 10 mM EDTA, pH 5.5 at 4°C overnight, to release the iron. The sample was then dialyzed extensively against 10 mM HEPES pH 7.0 at 4°C. SDS-PAGE was used to confirm the purity of the protein preparation.

TbpB-pTf Complex Formation

A 1.5:1 ratio of purified TbpB was added to holo-pTf in 10 mM HEPES, pH 7.0 buffer, and incubated for 1hr at room temperature. After incubation, the samples were applied to a Q-Sepharose anion exchange column. Only TbpB-Tf complex bound to the column and was eluted by the addition of 200 mM NaCl in the buffer. The pooled fractions were dialyzed extensively against 10 mM HEPES pH 7.0 at 4°C.

Mass shift analysis by hydrogen/deuterium exchange (H/DX)

Each H/DX experiment involved a measurement of deuteration levels for pTf, in the presence and absence of each of the four TbpB receptors. In this fashion, changes in deuteration arising from complexation could be used to identify the binding interface. These measurements were made using mass spectrometry of pTf peptides, generated by digesting deuterated protein under conditions preventing back-exchange of deuterium. Thus, these experiments provided a “peptide-level” resolution of binding interfaces and changes in protein dynamics resulting from binding.

Quadruplicate experiments were performed for each state (free or receptor-bound pTf). In

each experiment, protein stock solution was labeled at pH 7.0 in D₂O, (25% v/v) at 20°C for 2 minutes. The solution was then quenched and reduced on ice for 1.5 min (in 250 mM TCEP, 0.08% TFA (v/v), pH 2.3).

This quenched and reduced protein solution was digested with immobilized pepsin (Applied Biosystems) in a cartridge format (2.5 cm x 200 μm ID, assembled in-house). The digest was captured on a small C18 reversed-phase column and separated using a 5 to 90% steep linear gradient of acidified acetonitrile (0.03% TFA, 0.02% FA, all v/v). Effluent was directly infused into a QSTAR Pulsar *i* quadrupole time-of-flight (QqTOF) mass spectrometer. Digestion and chromatography were carried out in an ice bath.

In order to identify the pTf peptides arising from the digests, unlabeled peptides were prepared under similar conditions and sequenced by tandem mass spectrometry (MS/MS). The MS/MS spectra were searched against the pTf sequence using a local installation of Mascot 2.1, using conventional identification criteria. A total of 87 peptides were confirmed suitable for subsequent mass shift experiments.

Mass spectral data from each replicate H/DX-MS experiment was analyzed using Hydra v1.5 (36). The criteria used for determining significant mass shifts were described previously by Bennett et al (33). Briefly, significantly shifted peptides must meet the following criteria: a two-tailed t-test ($p < 0.05$) using pooled standard deviations from quadruplicate analysis of each state and receptor, and exceeding a threshold shift value (± 2 SD) based on a measurement of the shift noise and assuming a normal distribution. Deuteration data were then color coded blue and red for positive and negative shifts, respectively, and mapped to pTf structure (PBD 1H76).

Rosetta Docking

The Rosetta models used in this paper were generated as described by Moraes *et al.* (5) and Calmettes *et al.* (31). Briefly, the RosettaDock program was run in full atom mode using standard Monte Carlo movements, allowing for spin around the axis connecting the two proteins. Experimentally-determined important residues on the receptor-side only were taken into account during docking. Briefly, a program modification checked the RosettaDock-generated decoys for whether the residues designated were within 10Å of

pTf. Decoys that failed on any important residue were deleted. The program was then run continuously until all decoys met each of the designated TbpB distance constraints (31).

KFC Hot Spot Prediction

Rosetta docked models were submitted to the Mitchell lab KFC Hot Spot Prediction server, as described by Darnell et al. (37). The software combines two algorithms, K-FADE (Fast Atomic Density Evaluation) which measures shape specificity features, with K-CON, which uses biochemical contact features (37).

Surface Plasmon Resonance

Surface Plasmon resonance experiments were performed using a BiacoreX instrument (GE Healthcare) at 25°C, similar to those described by Calmettes et al. (31). Briefly, four pTf constructs (wild-type and pTf mutants D360A, R509A and S625K) were coupled to the sensor chip (research-grade CM5) via standard N-hydroxysuccinimide and N-ethyl-N-(dimethylaminopropyl) carbodiimide activation. TbpB orthologs (*ApH49*, *AsH57*, *ApH87* and *ApH89*) were diluted at various concentrations in the mobile phase buffer (10 mM Hepes, pH 7.5, 150 mM NaCl, and 0.005% (v/v) surfactant P20). Samples were injected at a flow rate of 20 µl/min, and bound receptor was subsequently removed by washing with mobile phase for 90 or 240 seconds after the injection. Regeneration buffer (10 mM Hepes, pH 7.5, 2 M NaCl) was injected prior to each analyte injection. Kinetic constants were calculated from the sensorgrams using the simulated BiacoreX evaluation software, version 4.0.1 (GE Healthcare).

SUPREX Analysis of FbpA

Apo FbpA was mixed 1:1 with the pTf-TbpB complex and incubated at room temperature with gentle rotation for 1 hour. A Microcon filtration device (Millipore USA, Billerica, MA) with a molecular weight cut-off (MWCO) of 50kDa was used to separate FbpA from the complex, followed by concentration with an Amicon 0.5 ml 10K MWCO Ultracel 10K membrane centrifugal concentrator (Millipore) (final concentration of 1mg/ml).

Apo FbpA, apo FbpA with complex, and holo FbpA were treated with increasing concentrations of Guanidine-hydrochloride (Gdn-HCl), from 0-4M, to generate a SUPREX denaturation curve in a manner similar to the

method described by Parker-Siburt et al. (13). The mass spectrometer used for detection is the same as described for the HD/X experiments. The Bayesian Protein Reconstruct application from BioAnalyst QSTM version 1.4 (Applied Biosystems) was used to deconvolute the acquired spectra, to generate average centroid masses for each of the labeled FbpA samples. A denaturation curve for each sample was then generated and fit using OriginPro version 8.

Absorption studies of FbpA

Apo FbpA was incubated with pTf-TbpB complex as described in the SUPREX experiment. A 50 kDa MWCO Microcon filter was used to separate FbpA from the pTf-TbpB complex. FbpA was then analyzed by spectrophotometry at 480 nm. Samples were prepared in triplicate, and related to controls (holo FbpA, apo FbpA and pTf-TbpB complex).

As an additional control, apo FbpA was incubated with FeCl₃ in 100 mM sodium bicarbonate, 100 mM sodium citrate, pH 8.6. Remaining free iron was removed via gel filtration chromatography, and the iron-loaded FbpA (apo FbpA + FeCl₃) was concentrated using an Amicon concentrator as described.

RESULTS

Mass shift perturbation mapping of bound and free porcine transferrin

The availability of structures for TbpB (5,31), and pTf (38) make this an ideal system for investigating the receptor-protein interaction. In this study, mass shift perturbation experiments (33) were carried out using TbpB's from four strains of the porcine pathogens *Actinobacillus pleuropneumoniae* (Ap) and *Actinobacillus suis* (As), to gauge intra-pathogen variability with respect to the pTf-TbpB interaction and to extend the previous analyses of human pathogenic receptor interactions (11).

Sequencing of peptides derived from pTf was performed as described by Ling *et al.* (11). A sequence coverage map for pTf can be found in **Figure S1**. In order to determine if a shift analysis of peptides from one large protein in the presence of another would be feasible, pTf and TbpB were processed simultaneously and the ability to detect pTf peptides in this mixture was determined with Hydra v1.5 and manual verification (36). While the complexity of the spectra increased significantly, there were few instances of peptide overlap and a

minimal impact of increased ion suppression on peptide detection. Collectively, the impact on pTf sequence coverage used in our mass shift studies was a reduction from 68% (98 peptides) in the absence of TbpB to 63% (87 peptides) in its presence. Surface and cartoon representations demonstrating the degree of sequence coverage are displayed in **Figure 1**, mapped onto the holo-pTf structure. Of the 18 disulfide bonds present in pTf (39), 15 peptides representing 8 disulfides were detected. This incomplete coverage is likely due to a combination of incomplete reduction under the conditions required to prevent deuterium back-exchange (most notably temperature and pH) and issues related to peptide detection. To ensure that the disulfide reduction was optimized for this application, extending the reduction time up to 10 min did not significantly increase the representation of cysteine-containing peptides (data not shown).

The extent of pTf peptide mass shifts, induced by binding each of the four TbpB variants was determined (**Figure 2**). The four receptor variants generated similar patterns of altered deuteration, with peptides showing significant changes relative to free pTf colored in red. All significant perturbations map to the C-lobe of pTf. None of the four receptor variants caused an increase in solvent accessibility upon pTf binding, as there were no significantly increased mass shifts. The significant changes were mapped to the C lobe of pTf for each receptor (**Figure 3**). These changes upon complexation can be attributed to newly-formed interfacial regions or localized stabilization of structure.

To confirm that these mass shifts were maximized, a saturation analysis was conducted in which shift measurements were monitored as a function of excess receptor. For example, shift values from pTf complexed with ApH87 TbpB in a 1:1 ratio were compared with similar analyses of pTf complexed with two-fold and four-fold excesses of the receptor. One-way ANOVA and Tukey tests confirmed that the shift values for each Tf peptide showed no significant change over this range, indicating that pTf was saturated with TbpB at the 1:1 ratio, as expected based upon the receptor

purification procedure (see Experimental Procedures).

This shift saturation provides the opportunity to compare regional differences in shift values across the receptor variants in greater detail (**Figure S2**). The pTf complexes with ApH49 and ApH87 receptor variants display the largest mass shifts in most affected regions of the C-lobe, and are for the most part equivalent within the error of the measurements. AsH57 is similar to these two variants, except for a weaker shift in peptides from 629-639. Finally, ApH89 shows the weakest set of shifts among all four receptors in this 629-639 region. Thus, while the shift measurements point to a commonly-affected region of pTf structure (**Figure 3**), there appears to be a moderate degree of variability in the sub-regions comprising elements of the heterodimer interface.

Correlation of mass shift perturbation data with binding site prediction

The computational docking of pTf to porcine TbpBs used structures for the ApH49 TbpB variant (5) and the AsH57 and ApH87 TbpB variants, as described in Calmettes *et al.* (31). There are currently no structures available for ApH89. The top scoring models for the three complexes were used to generate contact surfaces on pTf, representing the three TbpB-pTf interfaces. These contact surfaces highlight all residues on pTf within 5Å of the corresponding receptor (**Figure 4**). These surfaces define an interface spanning both C1 and C2 subdomains of the C-lobe that differ little among the variants in total surface area ($934 \pm 60 \text{ \AA}^2$).

The computational models in general support the findings of the shift analysis. TbpB docks with the C-lobe exclusively, in a manner bridging both C1 and C2 subdomains (interaction models of the remaining complexes can be found in **Figure S3**). Incomplete sequence coverage in the C2 lobe in particular prevents a full shift mapping of the interface, but the data do highlight a region spanning the two subdomains for ApH49 and ApH87, within the peptide resolution of the shift method. The remaining two receptors highlight a sub-lobe bias, *vide infra*. However, the independent empirical and computational approaches offer mutual support for localizing the binding domain to the C-lobe, generating a model of sufficient accuracy to direct a further validation through mutational analysis.

A knowledge-based “hot spot” prediction algorithm was applied to the heterodimer models (37). For the *ApH49* TbpB-pTf dimer, residues E508 and R509 on pTf were identified as key contributors to binding energy, based on both shape complementarity and chemical features of the contact, in a wider contact region that is essentially equivalent to the 5Å projection (**Figures 4 and S3**). These pTf hotspots are mirrored by two amino acid hotspots on *ApH49* TbpB (Y162 and F171). These two pTf residues demonstrate the strongest shape complementarity in the other two receptor-pTf complexes as well, although they fall just below the threshold for hotspots in the KFC model (37). For all three complexes, the remaining interfacial residues on pTf define a relatively homogenous contact surface with respect to shape and atomic interactions. This computational characterization does not suggest the insignificance of the remaining interfacial residues, rather that the protein-protein interaction is not dominated by hot-spots insofar as the computational method can identify them from a docked model.

Mutational Analysis of Binding Site

Several single amino acid mutations to pTf were then generated to test the proposed binding sites and to determine the significance of the predicted hot-spot and other residues at the interface. The mutations selected for quantitative analysis were based upon a scan of eight residues within the interface, using a simple affinity capture method involving *ApH49* TbpB (**Figure S4**). Only three mutations exhibited significant reductions in receptor binding via this method: D360A (C1-lobe, helix $\alpha 1$), S625K (C1-lobe, loop 23) and R509A (C2-lobe, loop 15). Designations of secondary structure follow the nomenclature of Hall *et al.* (38) and sublobes designations follow Hirose (40). R509 represents the putative hotspot, whereas D360 and S625 are oriented towards the receptor at the opposite end of the interface, and on the opposing subdomain of the pTf C-lobe (**Figures 4 and S3**).

Binding studies using surface plasmon resonance (SPR, BiacoreX) generated kinetics data for wild-type pTf and each of the three mutant pTf proteins to each of the four receptor variants (**Table 1** and **Figure S5**). Wild-type pTf

bound all four receptors with high affinity, generating K_d values consistent with previous measurements using isothermal calorimetry (i.e. 55 nM) (5). The data were conservatively fit using a 1:1 single-step binding model, but permitting heterogeneity. Direct immobilization can lead to a degree of variability in orienting the bound protein with respect to its cognate receptor, so this was considered the most appropriate model. A two-step model also provided a superior fit, however this was ruled out after noting that variable contact time with the receptor did not significantly alter the kinetics of dissociation. The data arising from the major component in the heterogeneous fit is presented in Table 1 as the most reliable means of comparing the effect of mutations on binding. We used heterogeneous modeling for all mutated pTf's as well, since these were immobilized in the same fashion as wild-type pTf.

These binding data show that the interaction is substantially weakened through a single mutation in the C2 sub-lobe. $\Delta\Delta G$ values range between 1.8 and 3.5 kcal/mol for the R509A mutation in loop 15, consistent with a hotspot. Mutations in the C1 sub-lobe had variable effects. A mutation in helix 1 (D360A) is strongly disrupting for variants *ApH49* and *ApH87*, but does little to weaken binding for *AsH57* and *ApH89*. A different region of the C1-lobe may compensate for these two, with an obvious candidate being loop 23 (**Figure 4**). However, a mutation in the C-terminal end of this loop (S625K) does not strongly affect binding for any of the four receptor variants we studied, but particularly for *ApH89*. Overall, these mutational data highlight a central role for the C2 sub-lobe in the interface, where R509 in particular may be classified as a hotspot. The data also suggest that the C1 sub-lobe plays a minor role in binding, but might contribute to high affinity interactions.

Stability analysis of bound vs. free pTf

Bridging two sub-lobes suggests a mechanism by which iron loading may influence the preference of TbpB for holo-pTf. To determine if an iron-dependent conformational change in pTf is required for receptor binding, we tested the effect of iron loading on pTf stability. Mass shift analysis using H/D exchange was used to compare holo and apo-pTf. Peptides with significantly-altered mass induced by iron coordination were identified using the same criteria as in the receptor study, and summarized in **Figure S6**. As expected, a large

number of overlapping peptide sequences show a decreased mass shift upon iron coordination, in both the N- and C-lobes. When mapped to the holo-pTf crystal structure (**Figure 5**), these peptides localize specifically to the known iron-coordination sites and an element of the C2-lobe (peptide 517-529, loop 15). However, iron unexpectedly induced an instability in two locations, shown as increased mass shifts upon iron coordination. One set of peptides localizes to the hinge region between the N- and C-lobes, suggesting that iron coordination induces greater flexibility between lobes. The other set is found in the C1-lobe (peptide 629-639, the C-terminal end of loop 23). In other words, iron coordination stabilizes one region critical for receptor binding (loop 15) but destabilizes a second region shown to be part of the interface (loop 23). Both of these regions can be stabilized upon binding, although loop 23 is the region where the variability among receptors was noted. The corresponding sequences in the N-lobe remain unchanged upon iron binding (**Figure 5**).

Since the regions involved in iron coordination did not display changes in mass upon receptor binding, this suggests iron retention. To verify this, we performed a SUPREX analysis of the complex in the presence of ferric binding protein A (FbpA), following established methods (13). Holo FbpA is known to be substantially more stable than apo FbpA, requiring higher concentrations of denaturant to induce unfolding (13). Thus, increased stabilization of FbpA in the presence of the TbpB-pTf complex would indicate the capture of free iron released by the complex. SUPREX analysis using 0-4M Gdn-HCl did not show any indication of iron capture by apo FbpA when incubated with the *ApH49* TbpB-pTf complex (**Figure S7a**). To confirm this finding, FbpA was isolated from solution (in the presence and absence of complex) and analyzed by spectrophotometry (**Figure S7b**). No absorption at 480 nm was observed as a result of co-incubation with the complex. Together, these results show that iron is retained in the TbpB-pTf complex.

DISCUSSION

Characterizing the interaction

Our analysis of the TbpB-pTf complex shows that an interaction with the C-lobe of transferrin is conserved, in spite of a considerable degree of sequence dissimilarity among the four receptor variants studied (31). The interaction can involve both sub-regions of the C lobe. Residue R509 on C2 is a hotspot for all receptor interactions, as is D360 on C1 for the two highest affinity receptors (*ApH49*, *ApH87*) (37). The computational approach only highlights R509, but this could be expected as the calculations are based on modeled structure. Nevertheless, identifying one of these sites through computation suggests a reasonably accurate mapping of the interfacial residues on transferrin, if not the actual high-resolution conformation. This level of accuracy awaits x-ray diffraction data from the crystallized complexes. The mass shift data, however, supports the conclusion that both sub-lobes are involved in the interaction with variants *ApH49* and *ApH87* (**Figure 3 and S2**).

For TbpB variant *ApH89*, the mutational and mass shift data together suggest an interaction favoring the C2 sub-lobe on pTf. Based on the SPR measurements, R509 contributes strongly to the interaction, but the mutated C1 residues do not. It may be that untested residues on the C1 sub-lobe contribute more to binding free energy, but a minor role for the C1 sub-lobe is supported by weak or absent mass shifts in the H/D analysis (**Figure 3 and S2**). Unfortunately a structure of this TbpB variant is not yet available, so at this stage we cannot determine the extent to which the interface departs from the three modeled in this study.

With respect to C1 sub-lobe involvement, variant *AsH57* is quite similar to *ApH89*. Its interaction is hardly altered by the D360A mutation in helix 1 (**Table 1**) and the C-terminal end of loop 23 does not become protected nearly as well as in the two highest affinity receptors (see **Figure S2**). It is not surprising that the loop may not have a critical role in receptor binding. It is strongly destabilized upon iron binding (**Figure 5**), suggesting an entropic penalty associated with engaging this region.

This conclusion is consistent with the structural classification of the receptors in the companion study (31). At the interface with pTf, *ApH49* and *ApH87* receptors are similar in the structure and

orientation of their cap region. In both cases, critical binding residues interact with loop 23. *AsH57* is structurally divergent in its cap region, presenting a much different interface. Although it appears to interact with the C-terminal element of loop 23, there are few obvious contacts in the docked model. The structure for *ApH89* is not available, but we tentatively classify it with *AsH57* based on limited or non-existent contact with the C1 sub-lobe. Taken as a whole, a high-affinity interaction with pTf requires binding to both sub-lobes but C1 may contribute to a minor degree, likely because of the large iron-induced destabilization of loop 23 in this region.

The unique conformational response of the C-lobe to iron loading is a surprising finding, given the strong structural similarity between the C and N-lobes, but this seems to support why TbpB is selective for the C-lobe. Aligning the two domains shows that the corresponding region on the N-lobe actually orients the regions of the proposed interface in a distinct fashion as well (**Figure S8**). Together, the binding region of the C-lobe is therefore structurally and conformationally distinct from the N-lobe.

Mechanistic and functional significance

In contrast to mammalian Tf receptors on host cells, which function through receptor-mediated endocytosis and rely on the acidification of the endosome to facilitate iron removal, bacterial receptors are responsible for extracting iron from Tf at the cell surface and transporting iron across the outer membrane. TbpB is a critical component in the recognition of the iron-loaded form of Tf (20,21) and is consistent across all variants studied in C-lobe targeting (11,31).

However, its role in iron release is not fully understood. Reporting on the interaction between human Tf and TbpB from human pathogens, Nemish *et al.* did not detect an independent role in iron release (41). It was suggested recently that both TbpA and TbpB can facilitate the transfer of iron from human Tf to FbpA in membranes isolated from *N. gonorrhoeae* (13). Our SUPREX and spectrophotometric data, based on sensitive measurements of iron scavenging using FbpA, shows that the isolated TbpB-pTf complex does not appear to influence iron release, supporting Nemish *et al.*, but a function involving the membrane environment cannot be ruled out.

The ability of TbpB to identify the iron-loaded form of the C-lobe may be advantageous under the conditions of the mucosal surface that these bacteria inhabit. Although there is no direct information on the states of Tf iron-loading at the mucosal surfaces, the monoferric C-lobe form was shown to be dominant in serum samples from different sites (42). The pH of the mucosal surface is slightly acidic, and since the monoferric C-lobe is relatively more stable than the N-lobe under conditions of lower pH, it is possible that the dominance of monoferric C-lobe is further enhanced at the mucosal surface.,

The results from this study therefore favor a model whereby TbpB functions to efficiently capture iron-loaded Tf regardless of the iron status of the host, for presentation to TbpA. This would generate efficient uptake since TbpA does not discriminate between apo or holo states (22,23). Further insights will require experiments involving TbpA and additional elements possibly involved in releasing iron from a TbpB-bound Tf state.

Our results also highlight a consistent binding motif on pTf, which seems to hold for human Tf and the corresponding human pathogens (11). While our companion study points to a degree of variability within the receptor binding site (31), the conserved nature of the Tf binding motif does suggest the existence of a reciprocally conserved epitope within the TbpB receptor. The current study therefore supports the pursuit of a broad-spectrum vaccine targeting TbpB, particularly when coupled with the general observation that TbpB is present in all clinical isolates .

REFERENCES

1. West, S. E. H., Sparling, P.F. (1985) *Infect. Immun.* **47**, 388-394
2. Schryvers, A. B., Morris, L.J. (1988) *Mol. Microbiol.* **2**, 281-288
3. Gray-Owen, S. D., Schryvers, Anthony B. (1995) *Infect. Immun.* **63**, 3809-3815
4. Schryvers, A. B., Stojiljkovic, I. (1999) *Mol. Microbiol.* **32**, 1117-1123
5. Moraes, T. F., Yu, Rong-hua, Strynadka, Natalie C.J., Schryvers, Anthony B. (2009) *Mol. Cell* **35**, 523-533
6. Mickelsen, P. A., Sparling, P.F. (1981) *Infect. Immun.* **33**, 555-564
7. Mickelsen, P. A., Blackman, E., Sparling, P.F. (1982) *Infect. Immun.* **35**, 915-920
8. Lee, B. C., Schryvers, A.B. (1988) *Mol. Microbiol.* **2**, 827-829
9. Dyer, D. W., West, E.P., Sparling, P.F. (1987) *Infect. Immun.* **55**, 2171-2175
10. Jacques, M. (2004) *Can. J. Vet. Res.* **68**, 81-85
11. Ling, J. M. L., Shima, C.H., Schriemer, D.C., Schryvers, A.B. (2010) *Mol. Microbiol.* **77**, 1301-1314
12. Cornelissen, C. N., Kelley, M., Hobbs, M.M., Anderson, J.E., Cannon, J.G., Cohen, M.S., Sparling, P.F. (1998) *Mol. Microbiol.* **27**, 611-616
13. Parker Siburt, C. J., Roulhac, P.L., Weaver, K.D., Noto, J.M., Mietzner, T.A., Cornelissen, C.N., Fitzgerald, M.C., Crumbliss, A.L. (2009) *Metallomics* **1**, 249-255
14. Schryvers, A. B., Gonzalez, G.C. (1990) *Can. J. Micro.* **36**, 145-147
15. Criado, M. T., Pintor, M., Ferreiros, C.M. (1993) *Res. Microbiol.* **144**, 77-82
16. Bobst, C., Zhang, Mingxuan, Kaltashov, Igor A. (2009) *J. Mol. Biol.* **388**, 954-967
17. Halbrooks, P. J., He, Qing-Yu, Briggs, Sara K., Everse, Stephen J., Smith, Valerie C., MacGillivray, Ross T.A., Mason, Anne B. (2003) *Biochem J.* **42**, 3701-3707
18. Bailey, S., Robert W. Evans, Richard C. Garratt, Beatrice Gorinsky, Samar Hasnain, Christopher Horsburgh, Harren Jhoti, Peter F. Lindley, J Assanah Mydin, Robert Sarra, and John L. Watson. (1988) *Biochemistry* **27**, 5804-5812
19. Giannetti, A. M., Halbrooks, Peter J., Mason, Anne B., Vogt, Todd M., Enns, Caroline A., Bjorkman, Pamela J. (2005) *Structure* **13**, 1613-1623
20. Boulton, I. C., Gorringer, Andrew R., Allison, Nigel, Robinson, Andrew, Gorinsky, Beatrice, Joannou, Christopher L., Evans, Robert W. (1998) *Biochem J.* **334**, 269-273
21. Renauld-Mongenie, G., Latour, Mireille, Poncet, David, Naville, Sophie, Quentin-Millet, Marie-Jose. (1998) *FEMS Micro. Lett.* **169**, 171-177
22. Retzer, M. D., Yu, Rong-hua, Schryvers, Anthony B. (1999) *Mol. Microbiol.* **32**, 111-121
23. Yu, R.-h., Schryvers, Anthony B. (1993) *Microb. Path.* **15**, 433-445
24. Krell. (2003) *J. Biol. Chem.* **278**, 14712-14722
25. DeRocco, A. J., Cornelissen, C.N. (2007) *Infec. Immun.* **75**, 3220-3232
26. Baltes, N., Hennig-Pauka, I., Gerlach, G-F. (2002) *FEMS Micro. Lett.* **209**, 283-287
27. Perkins-Balding, D., Ratliff-Griffin, M., Stojiljkovic, I. (2004) *Micro. Mol. Bio. Rev.* **68**, 154-171
28. Renauld-Mongenie, G., Poncet, David, Mignon, Michele, Fraysse, Sophie, Chabanel, Christophe, Danve, Bernard, Krell, Tino, Quentin-Millet, Marie-Jose. (2004) *Infect. Immun.* **72**, 3461-3470
29. Vonder Haar, R. A., Legrain, M., Kolbe, H.V.J., Jacobs, E. (1994) *J. Bacteriol.* **176**, 6207-6213
30. Alcantara, J., Yu, Rong-hua, Schryvers, Anthony B. (1993) *Mol. Microbiol.* **8**, 1135-1143
31. Calmettes, C., Yu, Rong-hua, Silva, Leslie P., Curran, David, Schriemer, David C., Schryvers, Anthony B., Moraes, Trevor F. (2011) *J. Biol. Chem.* **286**, 12683-12692
32. Mandell, J., G., Falick, Arnold M., Komives, Elizabeth M. (1998) *Proc. Natl. Acad. Sci. U. S. A.* **95**, 14705-14710
33. Bennett, M., Barakat, K., Huzil, T., Tuszynski, J., Schriemer, D.C. (2010) *Chem. Biol.* **17**, 725-734
34. Weiner, M. P., Costa, G.L., Schoettlin, W., Cline, J., Matthur, E., Bauer, J.C. (1994) *Gene* **151**, 119-123

35. Shouldice, S. R., Dougan, D.R., Skene, R.J., Tari, L.W., McRee, D.E., Yu, R-H, Schryvers, A.B. (2003) *J. Biol. Chem.* **278**, 11513-11519
36. Slysz, G. W., Percy, A.J., Schriemer, D.C. (2008) *Anal. Chem.* **80**, 7004-7011
37. Darnell, S. J., Page, David, Mitchell, Julie C. (2007) *Proteins* **68**, 813-823
38. Hall, D. R., Madden, J.M, Leonard, G.A., Bailey, S., Neu, M., Winn, M., Lindley, P.F. (2001) *Acta. Crys. Sec. D* **D58**, 70-80
39. Shen, Z. M., Yang, Jen Tsi, Feng, You-Min, Wu, Cheun-Shang C. (1992) *Prot. Sci.* **1**, 1477-1484
40. Hirose, M. (2000) *Biosci., Biotechnol., Biochem.* **64**, 1328-1336
41. Nemish, U., Yu, R.H., Tari, L.W., Krewulak, K. Schryvers, A.B. (2003) *Biochem. Cell Bio.* **81**, 275-283
42. Vogel, W., Herold, M., Margreiter, R., Bomford, A. (1989) *Klinische Wochenschrift* **67**, 538-542

FOOTNOTES

Acknowledgements

This research was funded with operating and infrastructure support provided by the Canadian Foundation for Innovation (CFI), the Canada Research Chair program, the Alberta Heritage Foundation for Medical Research (AHFMR), and the Canadian Institutes of Health Research (CIHR).

Abbreviations

Tf, transferrin; pTf, porcine transferrin; hTf, human transferrin; TbpB, Tf binding protein B; TEV, Tobacco Etch Virus; SDS-PAGE, sodium-dodecyl sulfate polyacrylamide gel electrophoresis; hydrogen/deuterium exchange mass spectrometry, H/DX-MS; transferrin binding protein A, TbpA; ferric binding protein A, FbpA; *Actinobacillus pleuropneumoniae*, Ap; *Actinobacillus suis*, As; stability of unpurified proteins from rates of H/D exchange, SUPREX; surface plasmon resonance, SPR; guanidine hydrochloride, Gdn-HCl.

Keywords

iron acquisition, transferrin, mass shift analysis, bacterial receptor, protein-protein interaction.

FIGURE LEGENDS

Figure 1. Structural representation of iron-loaded porcine transferrin. Figure highlights the sub-lobe designations (left) and a composite of the sequence coverage available in the mass shift experiments (right). Corresponding sub-lobes are colored sand (C2 and N1) and yellow (C1 and N2), with Fe³⁺ in red. Sequence coverage is shown in green. Structure based on PDB 1H76.

Figure 2. Mass shift values for pTf-TbpB interactions. Plots summarizes the mass shifts induced by interaction of holo-pTf with (A) ApH49 TbpB (B) ApH87 TbpB (C) AsH57 TbpB and (D) ApH89 TbpB. Significant alterations in peptide mass are represented as red bars, and insignificant shifts in green using criteria described by Bennett *et al.* (33). Dashed lines mark the 95% confidence interval for the null hypothesis. The positioning of the bars indicates the location of the pepsin-generated peptides in pTf sequence. All results from quadruplicate analyses

Figure 3. Superposition of the receptor-induced mass shifts on pTf structure. The figure maps the significant changes induced by (A) ApH49 TbpB (B) ApH87 TbpB (C) AsH57 TbpB and (D) ApH89 TbpB. Changes are mapped in red, and as they cluster in the C-lobe exclusively, only this region of pTf is

shown. Boxed region in (D) represents the C-terminal end of loop 23, not protected from exchange in the interaction with *ApH89* TbpB. The orientation of pTf used in Figure 1 is preserved.

Figure 4. Mapping of the proposed receptor interface on pTf. (A) Surface representation of pTf, oriented and color-coded as in Figure 1, with a projection of the *ApH49* TbpB interface highlighted in grey, based on a calculation of pTf residues within 5Å of the receptor. Sub-lobes are labeled as C2 and C1. (B) Selection of residues within the proposed receptor binding site for mutational analysis, representing each sub-lobe. (C) Orientation of *ApH49* TbpB relative to pTf, arising from a Rosetta-docking exercise guided by confirmatory mutations in TbpB (31). Pose is +90° relative to (A) and (B).

Figure 5. Superposition of the iron-induced mass shifts on pTf. Upon iron coordination, regions demonstrating increased protection are colored red, and those showing a decrease in protection are colored blue. The framed regions highlight changes that are unique to the C-lobe, where the C-terminal tail of loop 23 shows deprotection and loop 15 shows protection. Both regions were identified as elements of the TbpB binding interface (see Figures 2, 3).

TABLES

Protein	k_{on} ($M^{-1}s^{-1}$)	k_{off} (s^{-1})	K_d (nM)	$\Delta\Delta G$ (kcal/mol)
wild-type				
<i>ApH49</i>	1.75×10^5	7.7×10^{-3}	44 ± 1	-
<i>ApH87</i>	2.12×10^5	1.28×10^{-2}	60 ± 2	-
<i>AsH57</i>	2.52×10^5	3.06×10^{-2}	120 ± 4	-
<i>ApH89</i>	1.67×10^5	1.68×10^{-2}	100 ± 4	-
C1-lobe (D360A)				
<i>ApH49</i>	1.71×10^4	1.89×10^{-1}	$11,000 \pm 2000$	3.2
<i>ApH87</i>	1.83×10^4	4.12×10^{-2}	2200 ± 300	2.1
<i>AsH57</i>	1.44×10^5	5.34×10^{-2}	370 ± 19	0.6
<i>ApH89</i>	1.97×10^5	4.37×10^{-2}	222 ± 4	0.5
C1-lobe (S625K)				
<i>ApH49</i>	5.46×10^5	1.87×10^{-1}	343 ± 6	1.2
<i>ApH87</i>	2.02×10^5	8.28×10^{-2}	410 ± 8	1.1
<i>AsH57</i>	5.82×10^4	9.22×10^{-2}	1600 ± 100	1.5
<i>ApH89</i>	4.69×10^5	1.29×10^{-1}	275 ± 8	0.6
C2-lobe (R509A)				
<i>ApH49</i>	2.33×10^5	2.81×10^{-1}	1200 ± 100	1.9
<i>ApH87</i>	1.05×10^4	2.32×10^{-2}	2200 ± 200	2.1
<i>AsH57</i>	3.40×10^2	9.03×10^{-4}	2600 ± 100	1.8
<i>ApH89</i>	4.26×10^3	1.78×10^{-1}	$41,000 \pm 3000$	3.5

Table 1. Kinetic and thermodynamics of binding of pTf mutants to TbpB variants. The rate and dissociation constants were determined from sensorgrams involving the immobilization of pTf (wt and mutants) and the infusion of free TbpB variants. Data fit to a heterogeneous ligand binding model, and reporting only the major component of binding. $\Delta\Delta G$ values determined as $-RT\ln(K_{d,wt}/K_{d,mut})$.

Figure 1

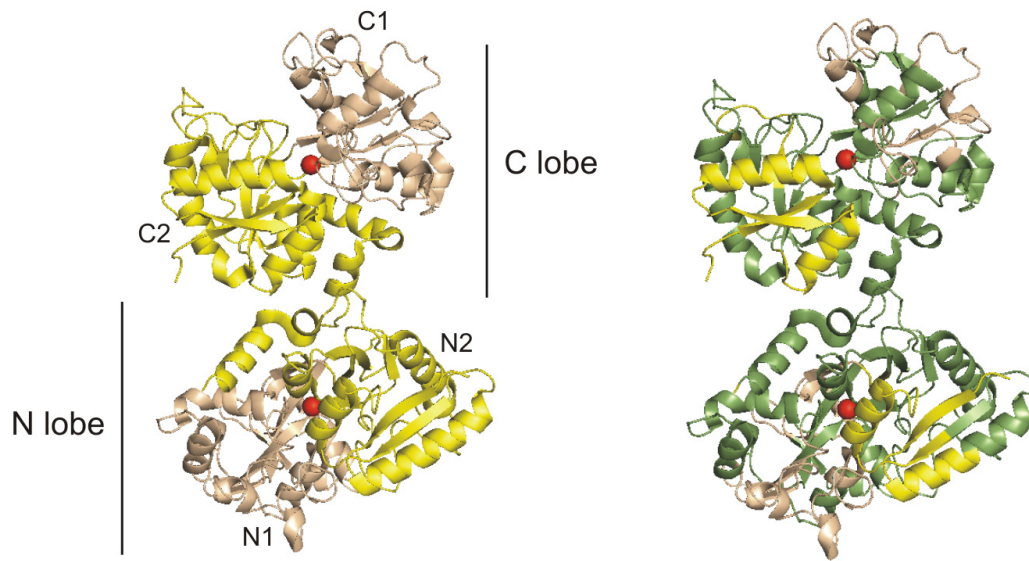


Figure 2

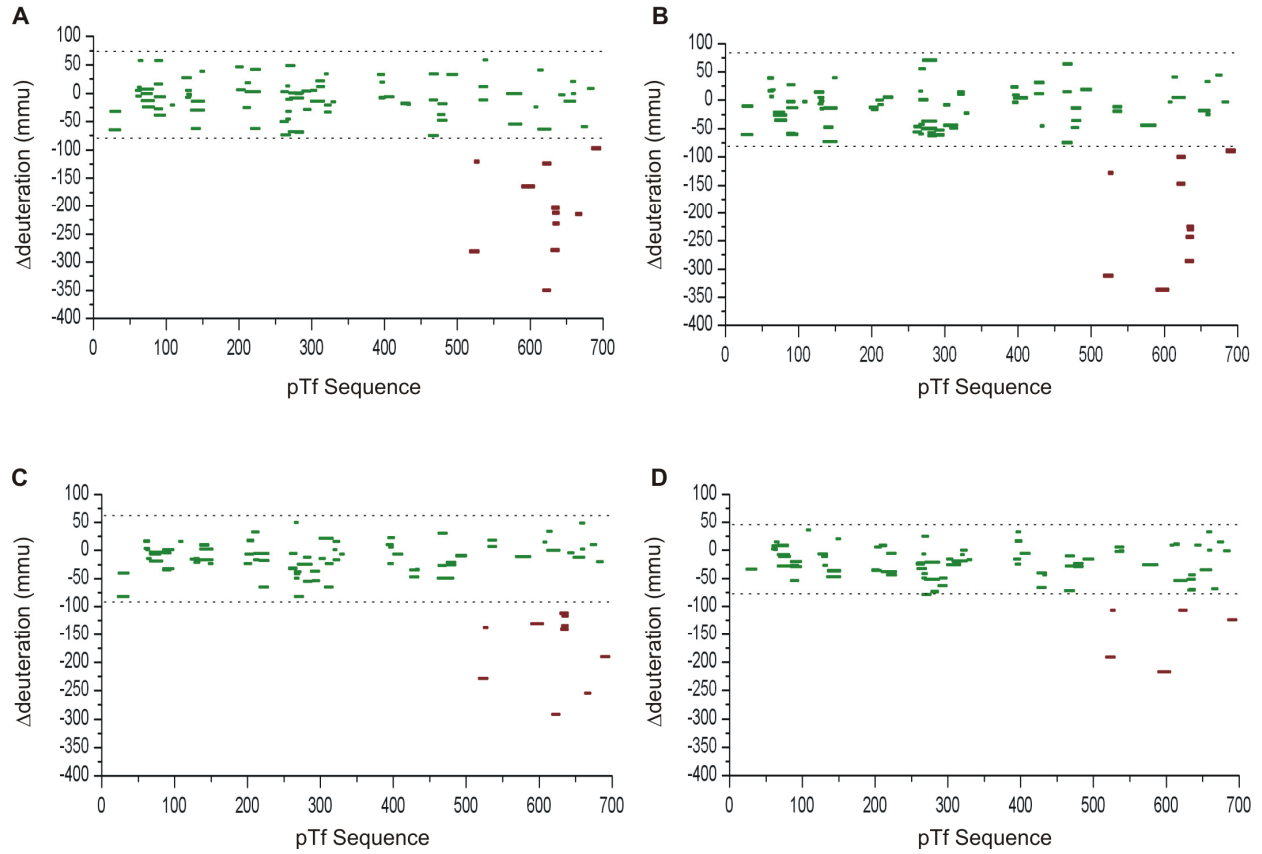


Figure 3

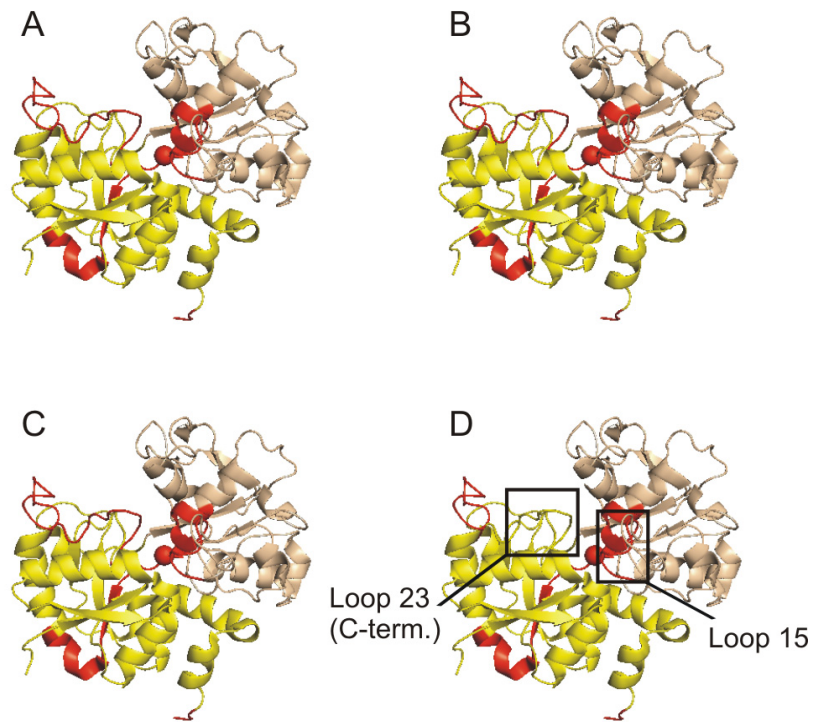


Figure 4

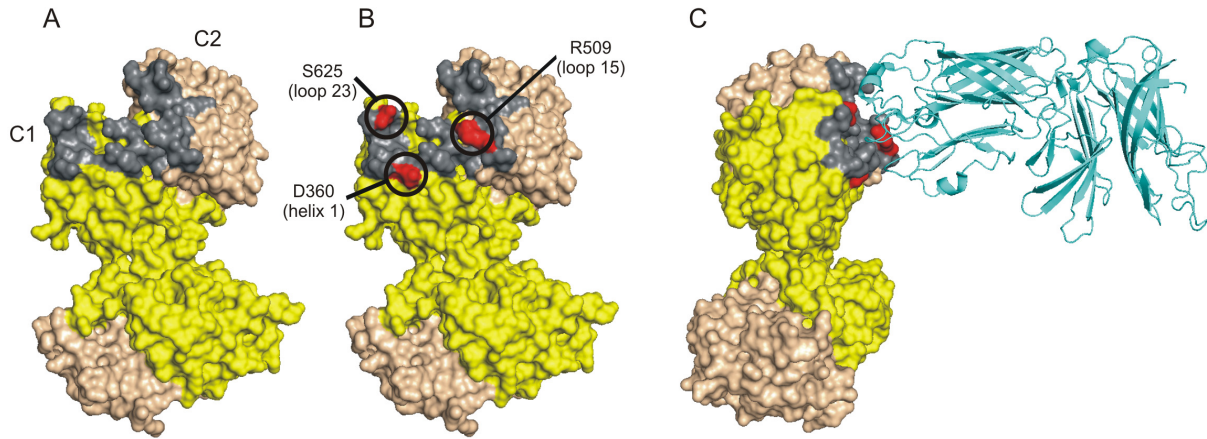


Figure 5

